Journal of Computational Physics 328 (2017) 344–353

Contents lists available at ScienceDirect

Journal of Computational Physics

www.elsevier.com/locate/jcp

Atom-partitioned multipole expansions for electrostatic potential boundary conditions

M. Lee [a,*], K. Leiter [a], C. Eisner [b,a], J. Knap [a]

[a] Simulation Sciences Branch, U.S. Army Research Laboratory, Aberdeen Proving Ground, MD 21005, USA
[b] Secure Mission Solutions, a Parsons Company, USA

ARTICLE INFO

Article history:
Received 25 February 2016
Received in revised form 23 September 2016
Accepted 5 October 2016
Available online 12 October 2016

Keywords:
Finite element method
Density functional theory
Spherical harmonics
Self-consistent field
Poisson equation
Partial differential equation
Quantum chemistry

ABSTRACT

Applications such as grid-based real-space density functional theory (DFT) use the Poisson equation to compute electrostatics. However, the expected long tail of the electrostatic potential requires either the use of a large and costly outer domain or Dirichlet boundary conditions estimated via multipole expansion. We find that the oft-used single-center spherical multipole expansion is only appropriate for isotropic mesh domains such as spheres and cubes. In this work, we introduce a method suitable for high aspect ratio meshes whereby the charge density is partitioned into atomic domains and multipoles are computed for each domain. While this approach is moderately more expensive than a single-center expansion, it is numerically stable and still a small fraction of the overall cost of a DFT calculation. The net result is that when high aspect ratio systems are being studied, form-fitted meshes can now be used in lieu of cubic meshes to gain computational speedup.

Published by Elsevier Inc.

1. Introduction

In chemical simulations, there are a variety of methods for computing the electrostatic energy of a real-space (non-periodic) charge density including pairwise Coulomb summation, fast multipole methods [1], and solving the Poisson equation [2,3]. Although fast multipole methods are being investigated [4] for grid-based real space density functional theory (DFT) [5], the most common method for computing electrostatics is the Poisson equation. Specifically, the electronic and nuclear charge densities are interpolated on a grid, and the electrostatic potential is solved via the linear Poisson equation [2]. In principle, the Poisson approach has linear scaling computational complexity because the kernel matrix is sparse with only $\mathcal{O}(N)$ non-zero matrix elements.

The Poisson equation requires specification of boundary conditions, such as a boundary potential (Dirichlet condition). Naïvely, the boundary values can be set to zero, but this can be a poor approximation for certain systems, such as those with a net charge (e.g., an ion) or those with a small amount of low-order multipolar content (e.g., a system with a net dipole). One method is to pad the grid with a large outer domain to ensure that the boundary values of the electrostatic potential, far away from the actual chemical system, are negligible [2]. Unfortunately, this approach can add significant computational expense by at least doubling the number of degrees of freedom.

In this study, we revisit the use of multipole expansions to estimate the electrostatic potential at boundary nodes [6–8]. This approach permits one to use a significantly smaller mesh while still providing accuracy commensurate with using an

* Corresponding author.
E-mail address: michael.s.lee131.civ@mail.mil (M. Lee).

http://dx.doi.org/10.1016/j.jcp.2016.10.012
0021-9991/Published by Elsevier Inc.

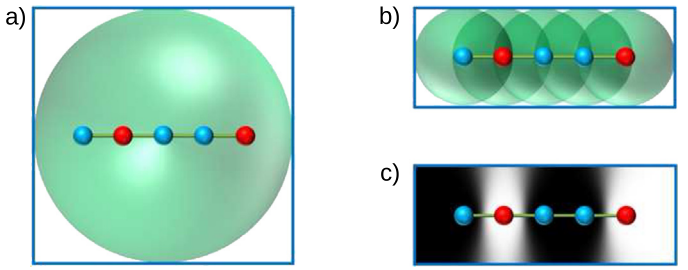

Fig. 1. (a) Schematic of a linear molecule embedded in a green sphere representing a single center domain for expanding exterior multipoles. (b) Same molecule embedded in atom-centered spheres, each delineating a separate exterior multipole expansion. (c) Illustration of the partition function used in this work (white = 1.0) for the two red atoms (2nd and 5th, from left to right) in the 1-D molecule. Blue box outlines represent the mesh boundaries where the electrostatic potential is approximated by multipole expansion. (For interpretation of the references to color in this figure, the reader is referred to the web version of this article.)

outer domain mesh. Traditionally, a single-center multipole expansion of the charge density has been used to estimate the boundary potential [7]. However, if one wishes to gain further computationally efficiencies with irregularly-shaped meshes (e.g., meshes fitted to high aspect ratio molecules), the single-center spherical (interior) multipole expansion can become problematic because it is technically incorrect in the situation where the potential is evaluated at a distance from the center closer than the some of the integrated charge density. In Fig. 1a, one can see that for a single-center expansion, a mesh (outlined in blue) must be large enough to encompass the multipole-interpolated charge domain (red). Therefore, multi-center multipole approaches have been proposed [9–12]. For example, Hirose et al. [12] divides the system domain into Voronoi polyhedra, whereby the charge density in each polyhedron is represented as a multipole expansion. Similarly, in this work, we build on the earlier works of atom-partitioned multipole expansions [9–12] and use normalized atom-centered radial-basis functions to define charge domains that are individually approximated by multipole expansions. When the charge domains are partitioned, such as by atom (Fig. 1b), then the overall mesh can be smaller and still encompass each charge domain. This algorithm can result in significant computational speedups for high aspect ratio systems, where we can now use smaller form-fitted meshes. Theory and methods are outlined in the next section and results are shown for various test cases.

2. Theory

2.1. Solving the Poisson equation by finite element method

The total electrostatic potential, $\phi(\mathbf{r})$, of a system with charge density, $q(\mathbf{r})$, can be obtained via solution of the linear Poisson equation [13],

$$-\frac{1}{4\pi}\nabla^2\phi(\mathbf{r}) = q(\mathbf{r}). \tag{1}$$

In DFT, specifically, the total charge density is a sum of electron and nuclear components,

$$q(\mathbf{r}) = \sum_{a=1}^{n_{atoms}} Z_a\delta(\mathbf{r}-\mathbf{R}_a) - \rho(\mathbf{r}), \tag{2}$$

where Z_a is the nuclear point charge, $\mathbf{R}_a$ is the atomic coordinate of atom a, and $\rho(\mathbf{r})$ is the electron density. In the finite element method (FEM), real space functions are interpolated on a grid of vertices (indexed as i) with shape functions, $N_i(\mathbf{r})$. For example, the electrostatic potential, ϕ, is represented as

$$\phi(\mathbf{r}) = \sum_{i=1}^{n_{nodes}} u_i N_i(\mathbf{r}). \tag{3}$$

The matrix form of the Poisson equation in finite element representation is [2]

$$\mathbf{Au} = \mathbf{b}, \tag{4}$$

where

$$A_{ij} = -\frac{1}{4\pi}\int_{\Omega} \nabla N_i(\mathbf{r})\cdot\nabla N_j(\mathbf{r})d^3\mathbf{r} \tag{5}$$

and

$$b_j = \int_\Omega N_i(\mathbf{r}) q(\mathbf{r}) d^3\mathbf{r}. \tag{6}$$

Regarding the nuclear component of $q(\mathbf{r})$ in Eq. (6), since nuclear charges are represented as delta functions, one can choose to ensure that they exactly coincide to a specific node and then increment the value of b at that node by the exact integral of the nuclear delta function, i.e. the nuclear charge. Typically, the total electrostatic energy of a system, E_{elec}, is the integral of the electron charge density and the electrostatic potential of the electrons and nuclei plus a classical nuclear–nuclear charge interaction term,

$$E_{elec} = \frac{1}{2}\int_\Omega q(\mathbf{r})\phi(\mathbf{r}) d^3\mathbf{r}.$$

However, there is a self-interaction term among nuclear charges that needs to be removed,

$$E_{self} = \frac{1}{2}\sum_{a=1}^{n_{atoms}} Z_a \phi^a_{self}(\mathbf{r}_a),$$

where each ϕ^a_{self} is computed from a distinct Poisson equation whereby a single nuclear charge, Z_a, is placed at $\mathbf{r}_a$ using the identical mesh for the full electrostatic problem. A further discussion of the self-energy removal procedure and its origin can be found in Ref. [2].

Given that the Poisson equation is a second order differential equation, boundary conditions must be specified, otherwise an infinite number of solutions to $\mathbf{u}$ are possible. For the nuclear self-interaction Poisson equations, it is efficient and accurate to assign boundary node values equal to the Coulomb potential of the single nuclear charge. However, for the full electrostatic system, the potential and potential gradient at the boundary nodes can be set to zero [2], while the outer grid is padded to a sufficient extent as to expect the actual boundary potential to be negligible. For systems with small or zero low-order multipoles (e.g., uncharged and no dipole), this may be a reasonable approximation. Nonetheless, padding adds extra degrees of freedom, slowing down not only the solution of the Poisson equation but also the rest of the DFT calculation.

2.2. Single-center multipole expansion of the charge density

Burdick et al. [7,14] show that the electrostatic potential can be approximated at the boundary of the inner domain, thus removing the need for an outer domain grid to capture the decaying potential. Furthermore, an estimated boundary potential would ensure that even the most diabolical situations (e.g., net-charged systems or systems with significant low-order multipoles) are handled correctly (i.e., up to a predictable error tolerance). We begin by noting that there is a Green's function solution to the Poisson equation,

$$\phi(\mathbf{r}) = \frac{1}{4\pi}\int_\Omega \frac{q(\mathbf{s})}{|\mathbf{r}-\mathbf{s}|} d^3\mathbf{s}. \tag{7}$$

The integral in Eq. (7) can be approximated via a single multipole expansion. First, we define a series of regular solid harmonics, S, of the form,

$$S_{lm}(\mathbf{r}) = Y_{lm}(\mathbf{r})|\mathbf{r}|^l, \tag{8}$$

where $Y_{lm}(\mathbf{r})$ are spherical harmonics,

$$Y_{lm}(\mathbf{r}) = (-1)^m \sqrt{\frac{2l+1}{4\pi}\frac{(l-m)!}{(l+m)!}} P_l^m(\cos\theta) e^{im\phi},$$

P_l^m is the associated Legendre polynomial [15] and indices l and m are restricted to $l >= 0$ and $|m| <= l$. When the expansion is centered at the origin, the conversion of $\mathbf{r} = r_x\hat{i} + r_y\hat{j} + r_z\hat{k}$ from Cartesian to spherical coordinates is

$$(r,\theta,\phi) = \left(|\mathbf{r}|, \arccos\left[\frac{r_z}{|\mathbf{r}|}\right], \arctan\left[\frac{r_y}{r_x}\right]\right). \tag{9}$$

The total multipole expansion of this system ($\mathbf{Q}$) is a sum of nuclear ($\mathbf{A}$) and electronic multipoles ($\mathbf{F}$),

$$Q_{lm} = A_{lm} + F_{lm}. \tag{10}$$

The nuclear multipoles, A_{lm}, are simply the sum of point charges multiplied by solid harmonics evaluated at the nuclear positions,

$$A_{lm} = \sum_{a=1}^{n_{atoms}} Z_a S_{lm}(\mathbf{R}_a). \tag{11}$$

The electronic multipoles are defined by integrals of the form,

$$F_{lm} = -\int_{\Omega} \rho(\mathbf{r}) S_{lm}(\mathbf{r}) d^3\mathbf{r}, \tag{12}$$

whereby the minus sign is due to the negative charge of an electron. These integrals can be evaluated by numerical quadrature, which is the standard machinery of FEM. Finally, the electrostatic potential at each boundary point, $\mathbf{r}_{i\in d\Omega}$, is estimated up to angular momentum order l_{max} as the sum of contributions from each charge multipole:

$$\phi(\mathbf{r}_{i\in d\Omega}) = \sum_{m=-l_{max}}^{l_{max}} \sum_{l=0}^{m} \frac{Q_{lm} Y_{lm}^*(\mathbf{r}_i)}{|\mathbf{r}_i|^{l+1}}. \tag{13}$$

This approximation, known as an exterior multipole moment expansion, is mathematically valid so long as $||\mathbf{r}_i||$ is greater than R, the radius of the charge integral domain Ω in Eq. (12). The multipole expansion method outlined above can be straightforwardly parallelized on multiple processors, since numerical integration of the solid multipoles and computation of the multipole-induced boundary potential values can be divided evenly among the processors in the same way that the finite elements are distributed. Besides our in-house FEM code, the above method (with some minor additions to correct for grid points outside a boundary sphere) has been implemented in various quantum codes such as the finite difference programs, PARSEC [6] and Octopus [8].

2.3. Atom-partitioned multipole expansions of the charge density

For anisotropic systems, form-fitted meshes such as rectangular prisms can be used to reduce mesh points/degrees of freedom and subsequently accelerate the DFT calculation. However, the exterior multipole moment expansion, in this case, would be no longer valid and may quickly become unstable. One way to manage an anisotropic mesh might be to consider also building an interior multipole moment expansion, whereby moments are computed by summations and integrals over inverse orders of $\mathbf{r}$, $\frac{1}{|\mathbf{r}|^{l+1}}$. Then, the electrostatic potential at different boundary nodes could be computed with either the interior or exterior moment expansion depending on its distance to the center. The problem we foresee with this approach, however, is that the singularities at the center of the interior multipole expansion due to inverse powers of $\mathbf{r}$ would be difficult to work around.

Therefore, we explored approximating the boundary potential via multipole expansions centered at each atom [9–12]. The general idea is to partition the charge density into atom-centered domains and represent each partitioned density as a multipole expansion centered at the parent atom (Fig. 1b). In order to ensure the sum of atomic-partitioned densities add up to the total charge density and every node's contributions add up to one, we use a partition of unity function:

$$U_a(\mathbf{r}) = \frac{B(\mathbf{r}-\mathbf{R}_a)}{\sum_{b=1}^{n_{atoms}} B(\mathbf{r}-\mathbf{R}_b)}, \tag{14}$$

where $B(\mathbf{r})$ is a radial basis function (RBF) that customizes the partitioning scheme. Partition of unity (also called "normalization" [12]) defined by Eq. (14) ensures that $\sum_{a=1}^{n_{atoms}} U_a(\mathbf{r}) = 1$ for all values of $\mathbf{r}$. There are many choices one can use for the RBF, including a Gaussian, an exponential, or a multi-quadric. From experimentation, we found the exponential RBF to work the best:

$$B(\mathbf{r}) = e^{-\gamma|\mathbf{r}|}, \tag{15}$$

where γ is an exponent parameter that can be tuned for accuracy (in this work, $\gamma = 3$). Mapping Eq. (15) on a 2-D plane for a hypothetical linear system, Fig. 1c shows how the normalized partition function causes the atom closest to the edge of the mesh to possess the entire edge of the mesh. In addition, the interior atom partitions a section of the mesh in between its two neighboring atoms. Analogous to Eq. (10), multipoles centered at atom a, Q_{lm}^a, are

$$Q_{lm}^a = A_{lm}^a + F_{lm}^a, \tag{16}$$

where the only non-zero component of the nuclear multipole is the monopole,

$$A_{00}^a = Z_a, \tag{17}$$

and the electronic multipole is weighted by the partition of unity function,

$$F_{lm}^a = -\int_{\Omega} \rho(\mathbf{r}) U_a(\mathbf{r}) S_{lm}(\mathbf{r}-\mathbf{R}_a) d^3\mathbf{r}. \tag{18}$$

The electrostatic potential at the surface due to atom-centered multipole expansions is an extension of Eq. (13),

$$\phi(\mathbf{r}_{i\in d\Omega}) = \sum_{a=1}^{n_{atoms}} \sum_{m=-l_{max}}^{l_{max}} \sum_{l=0}^{m} \frac{Q_{lm}^a Y_{lm}^*(\mathbf{r}_i-\mathbf{R}_a)}{|\mathbf{r}_i-\mathbf{R}_a|^{l+1}}. \tag{19}$$

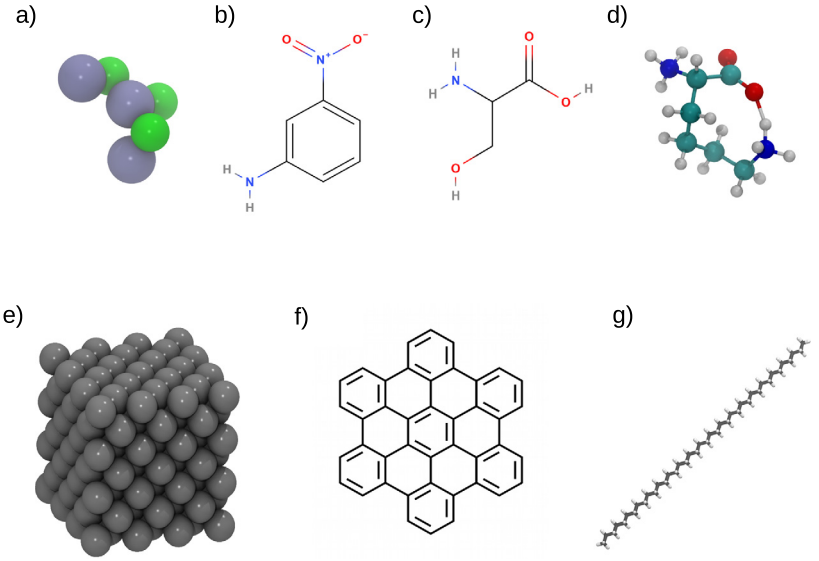

Fig. 2. Some of the systems investigated in this work: a) Li_3F_3 cluster (fluorine—green, lithium—blue), b) meta-nitroaniline, c) serine, d) lysine (zwitterion, +1 charge), e) aluminum $3\times3\times3$ cluster (Al_{172}), f) hexabenzocoronene (HBC, $C_{48}H_{12}$), and g) linear alkane (*trans* conformation, $C_{40}H_{82}$). (For interpretation of the references to color in this figure legend, the reader is referred to the web version of this article.)

While not considered here, choosing a compact RBF with C^2 continuity at its surface boundary would allow for reduced computational complexity in calculating Eqs. (17) and (18). In our implementation, we gain some speedup by first evaluating the partitioning function, $U_a(\mathbf{r})$, to determine if the multipoles, S_{lm}, even need to be computed for a given atom / quadrature point pair. However, Eq. (19) will still have complexity $\mathcal{O}([n_{nodes}]^{\frac{2}{3}} n_{atoms} l_{max}^2)$ unless one merges multipole expansions via a hierarchical scheme such as the fast multipole method [1]).

3. Methods

In this work, we implement and test the multipole expansion boundary potential algorithms with an in-house developed code that runs closed-shell real-space Kohn Sham density functional theory (KS-DFT) [2,16]. The exchange-correlation functional used is LDA, i.e., Perdew–Zunger [17]. We use a novel block variant of the Jacobi–Davidson method [18] (to be described in a future work) to solve the SCF eigenproblem. Spectral hexahedral $5\times5\times5$ (HEX125) finite element meshes [2] were constructed by a Python script interfacing Cubit version 13.2 [19]. The salient points of the mesh generation script are as follows. An inner domain cuboid of dimensions (L_x, L_y, L_z) is first constructed that encapsulates the entire chemical system with at least 8–12 bohr of vacuum in each Cartesian direction. For all-electron calculations, the mesh near each atomic center is subdivided four times using the local refinement algorithm in Cubit. Also, the grid point nearest to the atomic center is moved directly to that center, while neighbor nodes are partially dragged in the same direction. For the pseudopotential, valence electron-only metal cluster calculations, cubic $6\times6\times6$ spectral elements with side length equal to 1/4 of the lattice spacing were used. No local refinement was used for these meshes since the core electrons were excluded.

When an outer domain is specified, the inner domain cuboid is connected to an outer domain cube of side length, D. The six new hexahedra between the inner and outer domains are divided into a number of smaller hexahedra, balancing overall number of elements and elemental condition number. Specifically, the eight lines joining the corresponding vertices of the inner and outer domains are segmented into a geometric series of intervals, whereby each successive segment, starting from the outer domain, is 0.7 times smaller than the previous. The smallest segment is set to be roughly $4\times$ the length of the largest inner domain element size, s_{inner}. Given these constraints, the number of segments, n_{seg}, is estimated as

$$n_{seg} = \left\lfloor \frac{\log[1 - \frac{L_{outer}}{s_{inner}}(1-0.7)]}{\log 0.7} \right\rfloor, \tag{20}$$

where

$$L_{outer} = D - \frac{1}{3}(L_x + L_y + L_z).$$

4. Results and discussion

In order to analyze the two multipole approaches, we ran calculations on a variety of small molecules [20] shown in Fig. 2. As seen in Table 1, we used meshes that were sufficiently refined to yield basis-set completeness errors less than

Table 1
FEM vs. GAMESS (Gaussian basis set) energy.

Molecule	FEM outer domain padding, $B = 150$ bohr	FEM single center multipoles, $l_{max} = 12$	FEM atomic center multipoles, $l_{max} = 5$	GAMESS PCseg-4
Li_3F_3	−320.09254	−320.09241	−320.09241	−320.09231
m-Nitroaniline	−488.30676	−488.30655	−488.30655	−488.30589
Serine	−396.02576	−396.02575	−396.02575	−396.02517
Lysine	−493.00711	−493.47305	−493.47306	−493.47232

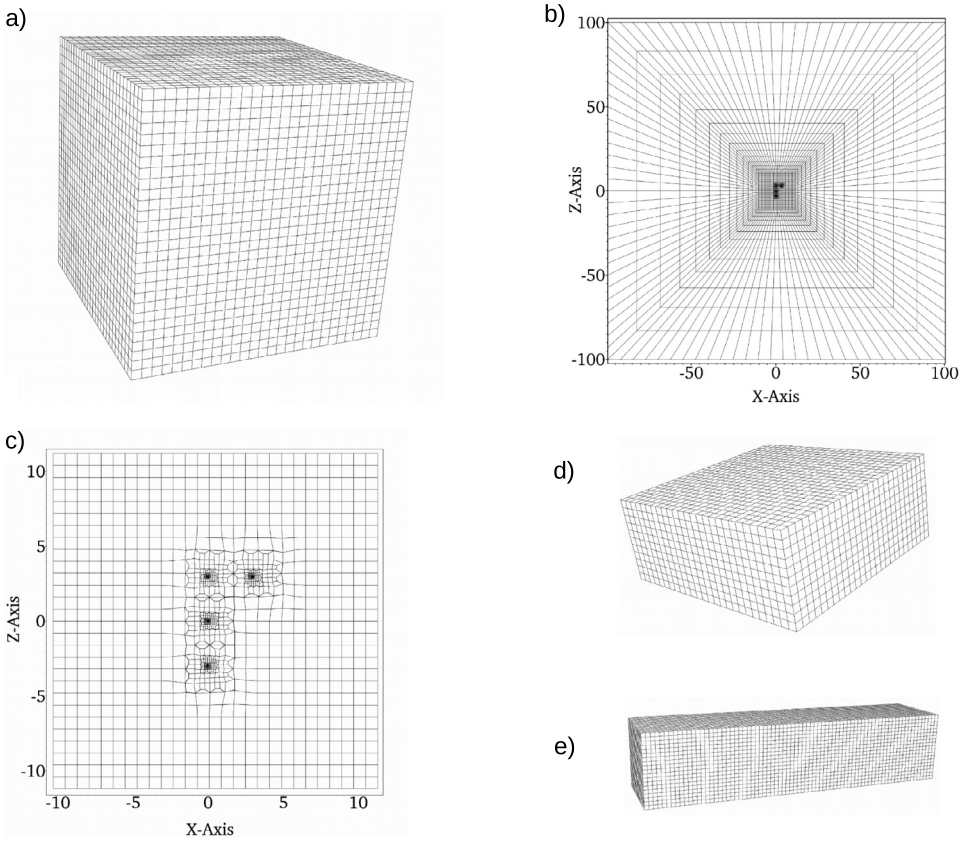

Fig. 3. a) Cubic mesh for Li_3F_3 encompassing both an inner and outer domain (side length = 100 bohr). b) Planar cross-section of this mesh showing a coarsened outer domain and a small and dense inner domain. c) Close-up of inner domain of this mesh whereby an 8-bohr buffer separates the atoms and the inner domain wall. Form-fitted meshes of d) hexabenzacoronene and e) $C_{40}H_{82}$ linear alkane.

1 mHartree when compared to the most complete Gaussian basis set available in the current version of GAMESS [21], PCseg-4 [22]. Accurate meshes were used to ensure both the correctness of the core FEM-DFT code and the multipole expansion module. We illustrate an example of a mesh that we used in Fig. 3 where HEX8 elements are displayed for clarity (HEX125 elements were used in the calculations). The cubic outer domain has a side length of 100 bohr for Li_3F_3 (Fig. 3a). A planar slice through the center of the cube (Fig. 3b) clearly indicates that the inner domain (central darker square) is a very small volume fraction of the overall system. Zooming in closer (Fig. 3c), the inner domain has a significant amount of padding (≥ 8 bohr from any atomic center) to accommodate for the tail of the valence electron density.

We explore two test systems in depth to determine how many multipoles are necessary to achieve converged results. In this work, we report the total SCF energy, but could have just as well reported electrostatic energy since >99% of the discrepancies between various the boundary/multipole methods reside in the electrostatic energy component alone. As can be seen in Figs. 4a and 4b, for meta-nitroaniline, 49 single-center multipoles ($l_{max} = 4$) are sufficient to achieve sub-mHartree accuracy vs. a benchmark calculation combining an outer domain ($B = 150$ bohr) and multipole expansion ($l_{max} = 12$). For the atom-centered multipole algorithm, considerably more multipoles (250) are required, corresponding to $l_{max} = 3$ expansions for each atom. Meanwhile, an outer domain of $B = 100$ bohr is required to reach sub-mHartree error (Fig. 4c). Similarly, for an ionic crystal cluster (Fig. 5), Li_3F_3, a single center with $l_{max} = 4$ (25 multipoles) yields

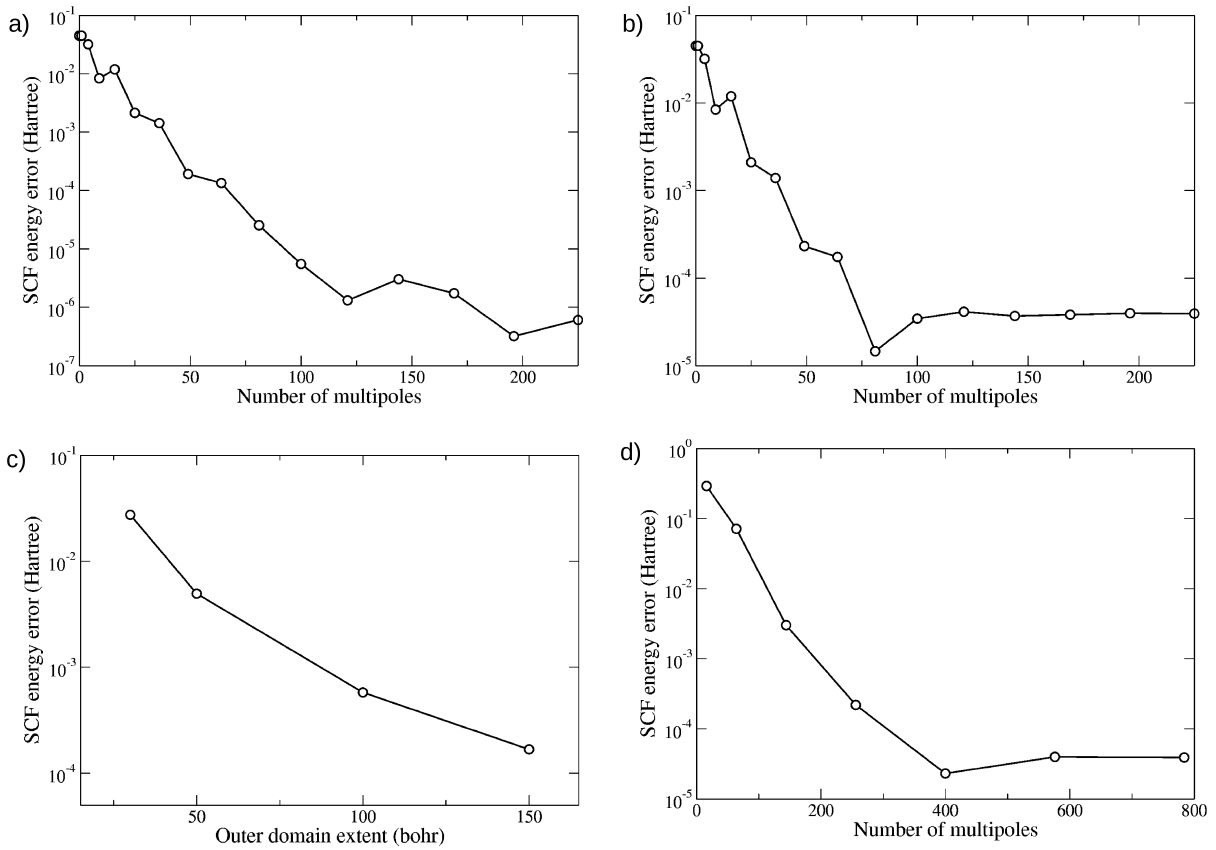

Fig. 4. Energetic accuracy of multipole and outer domain methods for meta-nitroaniline. a) SCF energy error of single center/no outer domain relative to single center/$l_{max} = 20$. b) SCF energy error of single center/no outer domain relative to benchmark of outer domain = 150 bohr and single center/$l_{max} = 12$. c) SCF energy error of outer domain/no multipoles relative to the same benchmark. d) SCF energy error of atomic centers/no outer domain relative to the same benchmark.

a sub-mHartree error vs. the benchmark calculation, while ≈50 multipoles with atomic centered multipoles, $l_{max} = 2$, is sufficient. Once again, an outer domain of $B \approx 100$ bohr is needed to ensure sub-mHartree agreement (Fig. 5c).

In Table 1, one can see that both the outer domain padding and the inner domain-only/multipole-expanded boundary potential yield similar results for the neutral systems we test. However, for the lysine system which has a formal charge of +1, the outer domain/no multipole result is incorrect. Addition of a monopole to the lysine/outer-domain system brings the energy in line with the other methods (−493.47312 Ha). Given that a outer domain extent of 150 bohr is sufficient for most molecular systems (except those with net charge), we compare number of mesh points and timings in Table 2. Generally speaking, we see that the multipole expanded boundary potential method leads to an entire SCF calculation being about twice as fast as one using an outer domain grid with a zeroed boundary potential. The benefit likely comes from cutting the number of grid points roughly in half. For finite difference codes (e.g., PARSEC [6] and Octopus [8]), we can only assume that multipole expansions have been a critical feature since a putative large outer domain grid would have been more costly in finite-difference without the ability to progressively coarsen the grid farther away from the center. Another common set of systems studied with real-space DFT codes are metal clusters. In Table 3, we look at an aluminum $3 \times 3 \times 3$ cluster (172 atoms, local evanescent pseudopotential [23], Fig. 2e) in comparison to the recent work of Motamarri et al. [2]. We compare a tiny outer domain ($B = 50$), which is equivalent to an ∼ 12 bohr vacuum inner domain, with a large outer domain ($B = 200$). As can be seen, a grid with a $B = 200$ bohr outer domain provides roughly the same result as a multipole-boundary enhanced 50 bohr outer domain with 2× reduced degrees of freedom and run-time.

For the meshes presented so far, the single center multipole expansion seems effective and sufficient for replacing the outer domain boundary. However, with highly non-isotropic grids (far from a sphere) and higher angular momentum expansions, the single-center method becomes invalid as discussed in Section 2.3. While meshes in our implementation of FEM KS-DFT must have non-jagged boundaries, we are free to use rectangular (right-angle) cuboids (prisms) as in Figs. 3d and 3e, which, in some cases, greatly reduce the number of nodes compared to a cube. To illustrate, we look at two high aspect ratio molecules embedded in form-fitting meshes: the 2-D graphene-like molecule, hexabenzocoronene (Fig. 2f, $C_{48}H_{12}$, "HBC") [24], in a flat mesh (Fig. 3d), and the linear alkane, $C_{40}H_{82}$ (Fig. 2g) [4], in a rod-shaped mesh (Fig. 3e). As one can see in Fig. 6a, the single-expansion SCF energies diverge for both of these systems as a function of multipole order. The

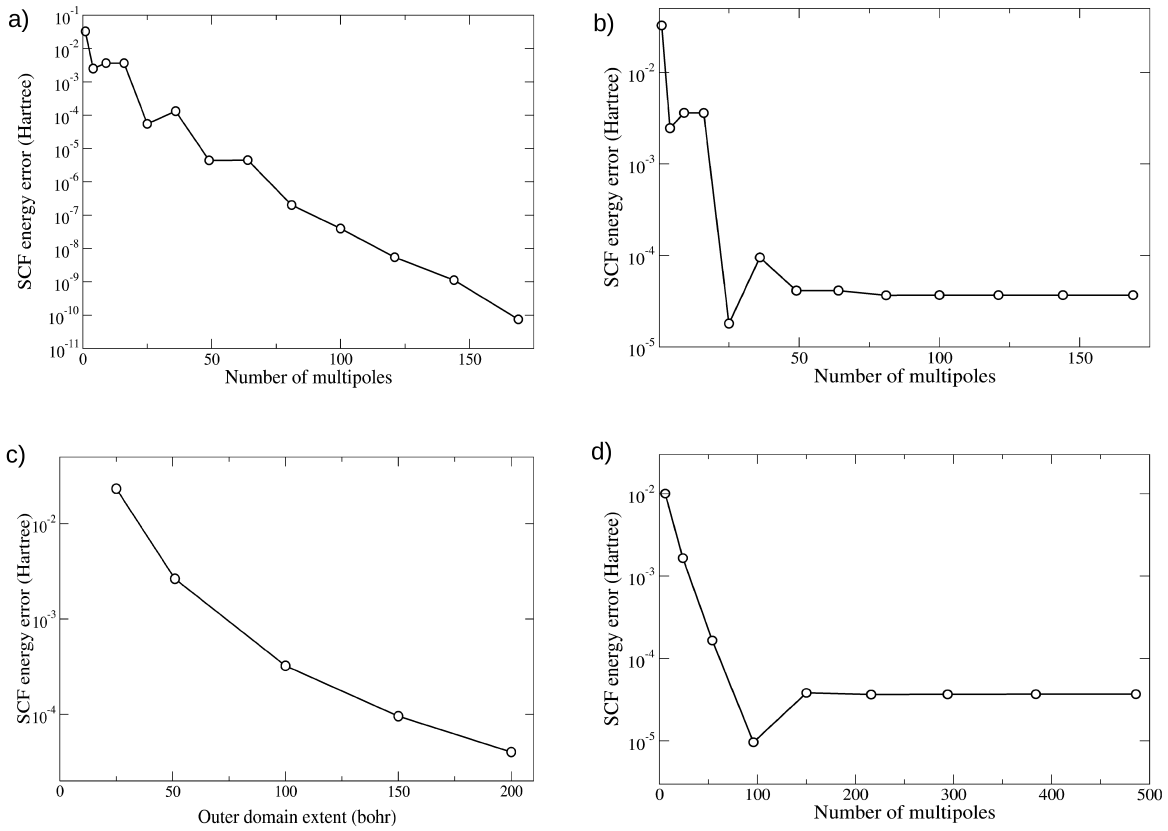

Fig. 5. Energetic accuracy of multipole and outer domain methods for Li_3F_3. a) SCF energy error of single center/no outer domain relative to single center/$l_{max} = 20$. b) SCF energy error of single center/no outer domain relative to benchmark of outer domain = 150 bohr and single center/$l_{max} = 12$. c) SCF energy error of outer domain/no multipoles relative to the same benchmark. d) SCF energy error of atomic centers/no outer domain relative to the same benchmark.

Table 2
Outer domain padding ($B = 150$ a.u.) vs. single ($l_{max} = 12$) and atomic center ($l_{max} = 5$) multipole expansions.

Molecule	Outer domain # nodes	Outer domain time (CPU-hrs)	Multipole expansion # nodes	Single center time (CPU-hrs)	Atomic centers time (CPU-hrs)
Li_3F_3	5,535,141	81	2,302,285	24	24
m-Nitroaniline	7,981,681	160	4,111,001	80	83
Serine	7,498,397	111	3,784,005	61	65
Lysine	10,814,273	212	6,135,401	143	159

Table 3
Aluminum $3 \times 3 \times 3$ cluster (172 atoms) with various boundary conditions.

Outer domain size (a.u.)	Boundary potential	#nodes	Time (CPU-hrs)	Energy/atom (eV)
50	zero	798,941	220	−56.03515
50	atomic ($l_{max} = 5$)	798,941	249	−56.01693
200	zero	1,681,001	486	−56.01666
200	atomic ($l_{max} = 5$)	1,681,001	475	−56.01635

graphs cannot be extended out because the calculations fail to run at higher multipole orders. Inspection of the boundary potential in Fig. 6c shows that the largest multipole-contributed boundary potential value grows with multipole order. The source of this behavior is likely due to the fact that spherical exterior multipole expansions are strictly valid only when the minimum radius of all of the potential evaluations is greater than the radius of the multipole integrals.

Meanwhile, Fig. 6b shows that our atomic multipole method has a stable reduction of error with increasing multipole order. Furthermore, while the largest potential values at the boundary are a bit high, they are constant regardless of multipole order. It is likely that the non-negligible potential values, here, are due to the fact that the atomic partitions are not

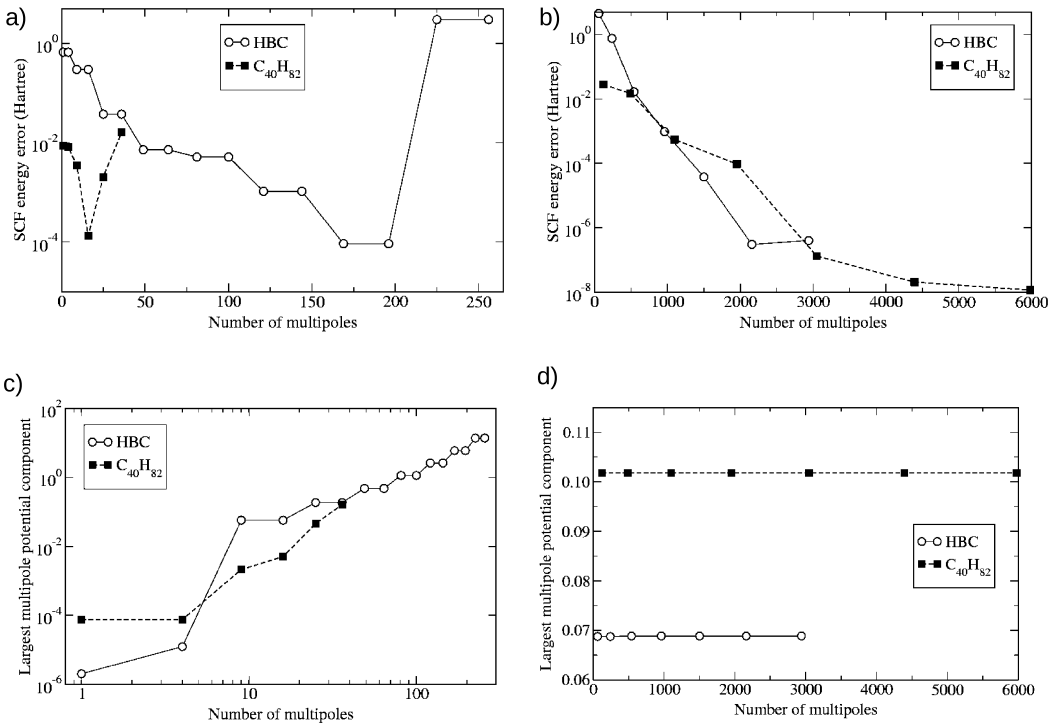

Fig. 6. Energetic accuracy of multipole and outer domain methods for hexa-benzocoronene (open circles) and $C_{40}H_{82}$ (*trans* conformation, closed squares). a) SCF energy errors of single center relative to atomic centers/$l_{max} = 6$. b) SCF energy errors of atomic centers relative to atomic centers/$l_{max} = 6$. c) Largest multipole contributions to a boundary potential node (single center). d) Largest multipole contributions to a boundary potential node (atomic centers).

Table 4
Comparison of size and CPU time for cubic and form-fitted meshes. Note: For alkane system, hexahedral $4 \times 4 \times 4$ spectral elements were used with only three levels of local refinement.

System	Cubic mesh # nodes	Cubic mesh (CPU-hrs)	Form-fitted mesh # nodes	Form-fitted mesh (CPU-hrs)
HBC	17,982,289	397	12,521,897	300
$C_{40}H_{82}$	17,537,614	594	5,842,228	196

actually spherical as caricatured in Fig. 1b. Instead, the partitions flow out to the edge of the mesh, as seen in Fig. 1c. We also suspect that this issue is mitigated by the fact that the electron density asymptotically decays exponentially and radially away from the atomic centers. In Table 4, we evaluate the computational efficiency achieved with using form-fitting meshes vs. "isotropic" cubic meshes. As one can see, we get a 30% benefit in timing by using a flatter box (Fig. 3d) for HBC and a substantial $3\times$ benefit for using a rod-like box (Fig. 3e) for $C_{40}H_{82}$. We expect similar gains for other irregularly-shaped systems like graphene nanoribbons, nanotubes, and other 1-D and 2-D systems.

5. Conclusion

Finite element formulations of density functional theory allow the use of a progressively coarsened outer domain to support the long-range tail of the electrostatic potential. However, in this work, we incorporate one or more multipole expansions to approximate the potential at the boundary so that a costly outer domain is no longer required. Compared to using an outer domain, multipole-expanded boundary potentials reduce the number of degrees of freedom in half and lead to DFT computations that are roughly twice as efficient. Furthermore, we re-introduce atomic-partitioned multipole expansions [9–12] which permit one to use irregular form-fitted meshes whereby the aspect ratios can deviate far from unity. This flexibility can lead to further 30% to 200% computational gains compared to having to use a cubic mesh. We surmise that our atomic-partitioned multipole expansion method should be generalizable to any grid-based linear PDE with atomic centers or reference points whereby the boundary conditions can be estimated by multipole expansions of the appropriate Green's function. Moreover, we conjecture that this method should be able to tolerate meshes more irregularly-shaped than rectangular prisms, so long as they roughly contour the system of interest.

Acknowledgements

We would like to thank C.X. Wang, V. Gavini, P. Motamarri, and B. Kanungo for helpful conversations. We would also like to thank the anonymous reviewers for making us aware of prior art. Computational time was provided the U.S. Army Research Laboratory, Navy, and Air Force DoD Supercomputing Resource Centers. Funding was provided by the ARL Computational Methods for Multiscale Modeling Program.

References

[1] H. Cheng, L. Greengard, V. Rokhlin, A fast adaptive multipole algorithm in three dimensions, J. Comput. Phys. 155 (2) (1999) 468–498.
[2] P. Motamarri, M.R. Nowak, K. Leiter, J. Knap, V. Gavini, Higher-order adaptive finite-element methods for Kohn–Sham density functional theory, J. Comput. Phys. 253 (2013) 308–343.
[3] L. Kronik, A. Makmal, M.L. Tiago, M. Alemany, M. Jain, X. Huang, Y. Saad, J.R. Chelikowsky, PARSEC—the pseudopotential algorithm for real-space electronic structure calculations: recent advances and novel applications to nano-structures, Phys. Status Solidi B 243 (5) (2006) 1063–1079.
[4] M. Zuzovski, A. Boag, A. Natan, An auxilliary grid method for the calculation of electrostatic terms in density functional theory on a real-space grid, Phys. Chem. Chem. Phys. 17 (47) (2015) 31550–31557.
[5] A.D. Becke, Basis-set-free density-functional quantum chemistry, Int. J. Quant. Chem. 36 (S23) (1989) 599–609.
[6] J.R. Chelikowsky, N. Troullier, Y. Saad, Finite difference pseudopotential method: electronic structure calculations without a basis, Phys. Rev. Lett. 72 (8) (1994) 1240.
[7] W.R. Burdick, Y. Saad, L. Kronik, I. Vasiliev, M. Jain, J.R. Chelikowsky, Parallel implementation of time-dependent density functional theory, Comput. Phys. Commun. 156 (1) (2003) 22–42.
[8] M.A. Marques, A. Castro, G.F. Bertsch, A. Rubio, Octopus: a first-principles tool for excited electron–ion dynamics, Comput. Phys. Commun. 151 (1) (2003) 60–78.
[9] M. Mezei, E.S. Campbell, Efficient multipole expansion: choice of order and density partitioning techniques, Theor. Chim. Acta 43 (3) (1977) 227–237.
[10] J.R. Rabinowitz, S.B. Little, Multipole expansion techniques for the calculation and characterization of molecular electrostatic potentials, Int. J. Quant. Chem. 30 (S13) (1986) 9–18.
[11] M. Berrondo, S. Eggleston, E. Larson, The effect of penetration on the multipole and multistreak expansions of molecular electrostatic potentials, Int. J. Quant. Chem. 36 (6) (1989) 749–764.
[12] K. Hirose, T. Ono, Y. Fujimoto, S. Tsukamoto, First-Principles Calculations in Real-Space Formalism: Electronic Configurations and Transport Properties of Nanostructures, World Scientific, 2005.
[13] P. Motamarri, M. Iyer, J. Knap, V. Gavini, Higher-order adaptive finite-element methods for orbital-free density functional theory, J. Comput. Phys. 231 (20) (2012) 6596–6621.
[14] S. Ghosh, P. Suryanarayana, SPARC: accurate and efficient finite-difference formulation and parallel implementation of density functional theory. Part I: isolated clusters, arXiv preprint, arXiv:1603.04334.
[15] J. Kurzak, B.M. Pettitt, Fast multipole methods for particle dynamics, Mol. Simul. 32 (10–11) (2006) 775–790.
[16] M. Lee, K. Leiter, C. Eisner, J. Crone, J. Knap, Extended Hückel and Slaters rule initial guess for real space grid-based density functional theory, Comput. Theor. Chem. 1062 (2015) 24–29.
[17] J.P. Perdew, A. Zunger, Self-interaction correction to density-functional approximations for many-electron systems, Phys. Rev. B 23 (10) (1981) 5048.
[18] G.L. Sleijpen, H.A. Van der Vorst, A Jacobi–Davidson iteration method for linear eigenvalue problems, SIAM Rev. 42 (2) (2000) 267–293.
[19] Cubit geometry and mesh generation toolkit, https://cubit.sandia.gov, 2013.
[20] S. Kim, P.A. Thiessen, E.E. Bolton, J. Chen, G. Fu, A. Gindulyte, L. Han, J. He, S. He, B.A. Shoemaker, et al., PubChem substance and compound databases, Nucleic Acids Res. (2015), http://dx.doi.org/10.1093/nar/gkv951.
[21] M. Schmidt, K. Baldridge, J. Boatz, S. Elbert, J. Gordon, M.S. Jensen, S. Koseki, N. Matsunaga, K. Nguyen, S. Su, T. Windus, M. Dupuis, J. Montgomery, General atomic and molecular electronic structure system, J. Comput. Chem. 14 (1993) 1347–1363.
[22] F. Jensen, Polarization consistent basis sets. II. Estimating the Kohn–Sham basis set limit, J. Chem. Phys. 116 (17) (2002) 7372–7379, http://dx.doi.org/10.1063/1.1465405.
[23] C. Fiolhais, J.P. Perdew, S.Q. Armster, J.M. MacLaren, M. Brajczewska, Dominant density parameters and local pseudopotentials for simple metals, Phys. Rev. B 51 (20) (1995) 14001.
[24] J.P. Hill, W. Jin, A. Kosaka, T. Fukushima, H. Ichihara, T. Shimomura, K. Ito, T. Hashizume, N. Ishii, T. Aida, Self-assembled hexa-peri-hexabenzocoronene graphitic nanotube, Science 304 (5676) (2004) 1481–1483.